

Article

Enhanced Detection Precision of the Taiji Program by Frequency Setting Strategy Based on a Hierarchical Optimization Algorithm

Jiafeng Zhang^{1,2}, Zhen Yang¹, Xiaoshan Ma^{1,3,*}, Xiaodong Peng^{1,4,5,6}, Chen Gao¹, Mengyuan Zhao^{1,2} and Wenlin Tang¹ 

- ¹ Key Laboratory of Electronics and Information Technology for Space System, National Space Science Center, Chinese Academy of Sciences, Beijing 100190, China
- ² University of Chinese Academy of Sciences, Beijing 100049, China
- ³ Institute of Engineering Thermophysics, Chinese Academy of Sciences, Beijing 100190, China
- ⁴ School of Fundamental Physics and Mathematical Sciences, Hangzhou Institute for Advanced Study, UCAS, Hangzhou 310024, China
- ⁵ Taiji Laboratory for Gravitational Wave Universe, Hangzhou 310024, China
- ⁶ Key Laboratory of Gravitational Wave Precision Measurement of Zhejiang Province, Hangzhou 310024, China
- * Correspondence: maxiaoshan@iet.cn

Abstract: For space-based gravitational wave detection, a laser interferometric measurement system composed of a three-spacecraft formation offers the most rewarding bandwidth of astrophysical sources. There are no oscillators available that are stable enough so that each spacecraft could use its own reference frequency. The conversion between reference frequencies and their distribution between all spacecrafts for the synchronization of the different metrology systems is the job of the inter-spacecraft frequency setting strategy, which is important for continuously acquiring scientific data and suppressing measurement noise. We propose a hierarchical optimization algorithm to solve the frequency setting strategy. The optimization objectives are minimum total readout displacement noise and maximum beat-note frequency feasible range. Multiple feasible parameter combinations were obtained for the Taiji program. These optimized parameters include lower and upper bounds of the beat note, sampling frequency, pilot tone signal frequency, ultrastable clock frequencies, and modulation depth. Among the 20 Pareto optimal solutions, the minimum total readout displacement noise was $4.12 \text{ pm}/\sqrt{\text{Hz}}$, and the maximum feasible beat-note frequency range was 23 MHz. By adjusting the upper bound of beat-note frequency and laser power transmitted by the telescope, we explored the effects of these parameters on the minimum total readout displacement noise and optimal local laser power in greater depth. Our results may serve as a reference for the optimal design of laser interferometry system instrument parameters and may ultimately improve the detection performance and continuous detection time of the Taiji program.

Keywords: frequency distribution scheme; Taiji program; hierarchical optimization algorithm; laser interferometry system



Citation: Zhang, J.; Yang, Z.; Ma, X.; Peng, X.; Gao, C.; Zhao, M.; Tang, W. Enhanced Detection Precision of the Taiji Program by Frequency Setting Strategy Based on a Hierarchical Optimization Algorithm. *Sensors* **2023**, *23*, 9431. <https://doi.org/10.3390/s23239431>

Academic Editor: Lei Huang

Received: 12 October 2023

Revised: 20 November 2023

Accepted: 22 November 2023

Published: 27 November 2023



Copyright: © 2023 by the authors. Licensee MDPI, Basel, Switzerland. This article is an open access article distributed under the terms and conditions of the Creative Commons Attribution (CC BY) license (<https://creativecommons.org/licenses/by/4.0/>).

1. Introduction

In 2016, the Laser Interferometer Gravitational-Wave Observatory (LIGO) [1] successfully detected gravitational wave phenomena that proved the existence of gravitational waves. Space-based gravitational wave detection missions have been proposed and performed in recent years because of the surface vibrations of the Earth, the noise of the gravitational gradient, and limitations of the ground test baseline length [2]. These missions include the Laser Interferometer Space Antenna (LISA) mission [3,4] and the Taiji [5–7] and Tianqin programs [8]. Space-based gravitational-wave detection usually uses the laser interferometry principle [9] and employs a three-spacecraft constellation placed in an equilateral triangle [3–6,8]; many functions are achieved by laser beams exchanged between

the spacecrafts (S/Cs), such as scientific interferometry, absolute inter-spacecraft distance measurements, digital data communication, and clock-noise transfer [10–12].

In a three-spacecraft constellation, the laser on one S/C interferes with the laser received from another S/C. The beat-note signal of two laser is digitized by an analog-to-digital converter (ADC) and analyzed by a high-precision phasemeter (PM). Both the ADC and the PM are triggered by an ultrastable oscillator (USO) that provides a time reference. The frequency instability of the trigger signal introduces additional ranging noise, affecting the arm length measurements. Additionally, the inherent jitter of the ADC distorts the sampling process. A pilot tone (i.e., a stable sinusoidal reference signal derived from the USO) has been inserted to correct the clock and ADC noise [6,13,14]. Considering the differential jitter and relative drift of three onboard USOs on different S/Cs, a clock-tone transfer chain has been proposed via an electro-optic modulator (EOM) to modulate the USO signal to sidebands on the outgoing beam to remove clock noise and correct the relative clock drift by using postprocessing [10–12]. To realize the functions listed above, the frequencies of the USO, sideband, pilot tone, ADC sampling, and beat note must be comprehensively considered and optimized. Moreover, total laser power is a limited resource used to ensure the effectiveness of scientific signal interference, and the readout displacement noise of the signal is affected by the power ratio of the sideband and carrier. The power ratio needs to be reasonably designed to minimize readout displacement noise.

Different frequency-setting schemes have been established for the LISA mission to address different concerns. For example, Kullmann [15] conducted a detailed, in-depth device experiment for the setting of the ADC sampling and pilot-tone frequencies involved in the LISA mission. They concluded that when the pilot-tone frequency was 72 MHz and the ADC sampling frequency was 50 MHz, sampling the beat-note frequency from 2 to 20 MHz could meet the noise requirements of this component of LISA. Barke [13] designed an inter-satellite frequency distribution scheme for the LISA program for beat-note frequencies in the range of [7 MHz, 23 MHz]; the ADC sampling and pilot-tone frequencies were 80 and 75 MHz, respectively. Zhang [16] analyzed the Taiji mission orbit and a possible phase-locking scheme and developed an offset frequency-setting scheme for beat-note frequencies in the range of [5 MHz, 25 MHz]. Although all these schemes have considered the problem of frequency setting in space-based gravitational-wave detection missions from different perspectives, they have not provided complete constraints or optimal setting schemes that include the beat-note frequency range as well as the frequencies of USO, ADC sampling, pilot tone, and sideband, and none of them consider the coupling relationship between frequency parameters. The unified consideration of these factors avoids the one-sidedness of individual parameter settings and reduces unnecessary redundancy between parameters, further improving the detection capability.

In this study, a frequency distribution scheme using a hierarchical optimization algorithm is introduced for the Taiji program by considering the frequency bands or frequencies for each function or device to ensure an accurate readout of the inter-spacecraft heterodyne signal, synchronize the onboard clock with those on other S/Cs, and generate an ADC sampling frequency and pilot tone signal.

The remainder of this paper is organized as follows. Section 2 introduces frequency factors and constraints, such as sideband frequency, ADC sampling, and pilot-tone frequencies. The optimization algorithm is introduced in Section 3. Section 4 describes the solution for the frequency setting scheme for each function or device. The effects of key parameters and total readout displacement noise are also analyzed. Finally, Section 5 concludes this study.

2. Frequency Factors and Constraints

In space-borne, gravitational-wave detection missions, laser links need to accomplish ultralong-range laser interference and various auxiliary functions, such as clock-noise transfer, pseudorandom noise (PRN) ranging, and information transfer [10,17]. The Doppler shift affects the beat-note signal generated by heterodyne interference; therefore, offset

frequencies need to be added to the phase-locking process to make them fall into a reasonable range. The signal is sampled and analyzed by the ADC and PM and triggered by the USO onboard. The USO signal is first multiplied to the GHz level and imprinted on the sidebands of the outgoing laser beam by EOM to perform inter-spacecraft clock transfer. Setting the sideband frequency and power ratio will affect the size of the readout displacement noise. The USO is then multiplied to the MHz level to provide the internal clock signal for the ADC and PM operations and construct the pilot tone to eliminate ADC sampling jitter and clock noise. In this process, some parameters have complex mutual constraints and need to be optimized systematically.

2.1. Readout Displacement Noise and Sideband Frequency Constraints

The Taiji program requires that the total readout displacement noise be as small as possible, which includes carrier and first-order sideband readout displacement noise. Moreover, based on the experience of the LISA mission [13,14,18], the first-order sideband readout displacement noise cannot be higher than 1/10 of the total readout displacement noise. The power ratio between the first-order sidebands and carrier could be expressed by the ratio of the squares of first- and zero-orders of the Bessel functions of the first kind:

$$\frac{P_{\text{sideband}}}{P_{\text{carrier}}} = \frac{J_1(m)^2}{J_0(m)^2}, \quad (1)$$

where $J_0(m)$ and $J_1(m)$ denote the zero- and first-orders of the Bessel functions of the first kind, respectively, and m is the modulation depth. Research on the LISA mission [14,18] indicates that this power ratio should be in the range of 5% to 10%, and that the corresponding modulation depth m is in the range of [0.44, 0.61], as shown in Figure 1.

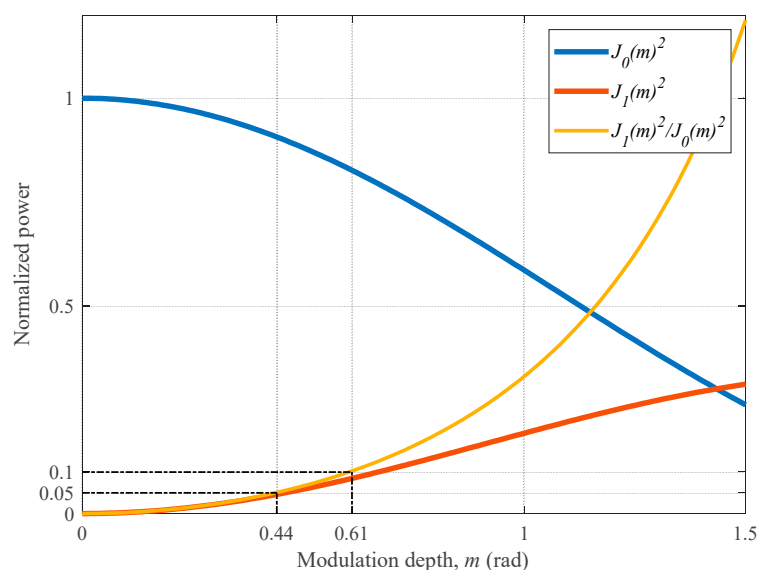


Figure 1. Carrier, first-order sideband (normalized power over the modulation depth m), and the ratio between the first-order sideband and carrier.

Therefore, the optimization objective and constraints are

$$\begin{aligned} & \text{Min}(\delta x^{\text{total}}) \\ & \left\{ \begin{array}{l} \delta x^{\text{sideband}} < \frac{1}{10} \delta x^{\text{total}} \\ 0.44 < m < 0.61 \end{array} \right. , \quad (2) \end{aligned}$$

where $\delta x^{\text{sideband}}$ and δx^{total} indicate the sideband and total readout displacement noise, respectively. The expressions of the readout displacement noise of the carrier and first-order sideband and the total readout displacement noise are [13]

$$\begin{cases} \delta x^{\text{carrier}} = \frac{\lambda}{2\pi} \frac{1}{J_0(m)^2} \delta \phi_{\text{total}} \\ \delta x^{\text{sideband}} = \frac{1}{\sqrt{2}} \frac{\lambda}{2\pi} \frac{f_{\text{het}}}{f_{\text{USO}}} \frac{1}{J_1(m)^2} \delta \phi_{\text{total}} \\ \delta x^{\text{total}} = \delta x^{\text{sideband}} + \delta x^{\text{carrier}} \end{cases}, \quad (3)$$

respectively, where λ is the laser wavelength, which is 1064 nm in the Taiji program; f_{het} is the beat-note frequency; and f_{USO} is the USO frequency. Given that two identical sidebands are generated on the left- and right-hand sides of the carrier after modulation by EOM, a factor of $1/\sqrt{2}$ must be added to the calculation of the sideband frequency noise. $\delta \phi_{\text{total}}$ is the total readout phase noise and contains three components, which is shown as follows [13,19]:

$$\begin{cases} \delta \phi_{\text{total}} = \sqrt{\delta \phi_{\text{SN}}^2 + \delta \phi_{\text{RIN}}^2 + \delta \phi_{\text{EN}}^2} \\ \delta \phi_{\text{SN}} = \sqrt{\frac{2e(P_{\text{local}} + P_{\text{receive}})}{R_{\text{pd}} \epsilon_{\text{het}} P_{\text{local}} P_{\text{receive}}}} \\ \delta \phi_{\text{RIN}} = \text{RIN} \sqrt{\frac{P_{\text{local}}^2 + P_{\text{receive}}^2}{2\epsilon_{\text{het}} P_{\text{local}} P_{\text{receive}}}} \\ \delta \phi_{\text{EN}} = \frac{\sqrt{2N_{\text{pd}}}}{R_{\text{pd}}} \sqrt{\frac{\delta I_{\text{pd}}^2 + 2\pi C_{\text{pd}} f_{\text{upper}} \delta U_{\text{pd}}}{\epsilon_{\text{het}} P_{\text{local}} P_{\text{receive}}}} \end{cases}, \quad (4)$$

where $\delta \phi_{\text{SN}}$, $\delta \phi_{\text{RIN}}$, and $\delta \phi_{\text{EN}}$ are the shot, RIN, and electronic noise, respectively; and P_{local} and P_{receive} represent the local laser power and laser power received by the telescope, respectively. P_{receive} [12] is calculated as

$$P_{\text{receive}} = 0.4073 \times \frac{\pi^2 D^4 P_{\text{tel}} \epsilon_{\text{opt}}}{8L^2 \lambda^2}. \quad (5)$$

For the Taiji program, the explanation and values of other parameters in Equations (4) and (5) are listed in Table 1.

Table 1. Taiji program parameters.

Parameter	Symbol	Value
Electron charge constant	e	$1.6 \times 10^{-19} \text{ C}$
Heterodyne interference efficiency	ϵ_{het}	0.8 [20]
Photodiode responsivity	R_{pd}	0.68 A/W [20]
Relative intensity laser noise	RIN	1×10^{-8} [21]
Photodetector phase number	N_{pd}	4
Photodetector voltage noise	δU_{pd}	2 nV/ $\sqrt{\text{Hz}}$
Photodiode capacitance	C_{pd}	10 pF
Current noise	δI_{pd}	1.5 pA/ $\sqrt{\text{Hz}}$ [22]
Laser power transmitted through the telescope	P_{tel}	2 W [7]
Total optical efficiency	ϵ_{opt}	0.853 [23]
Arm length	L	$3 \times 10^9 \text{ m}$ [6]
Diameter of telescope	D	40 cm [7]

In Equation (3), $\delta x^{\text{sideband}}$ is positively correlated with f_{het} and negatively correlated with f_{USO} . Because the beat-note frequency signal f_{het} varies with time, $\delta x^{\text{sideband}}$ is usually calculated by replacing f_{het} with f_{upper} . From Equations (3) and (4), the total

readout displacement noise may be minimized by reasonably setting f_{upper} , f_{USO} , m , P_{receive} , and P_{local} .

2.2. Constraints of the ADC Sampling and Pilot-Tone Frequencies with the Beat-Note Frequency

According to Nyquist's theorem, the sampling frequency of the ADC needs to be greater than at least two times the beat-note frequency. That is,

$$f_{\text{ADC}} > 2f_{\text{upper}}. \quad (6)$$

The USO is used to control the ADC sampling frequency and construct the pilot-tone signal; the divider or synthesizer can realize this process. According to Heinzl [10], the noise introduced by the dividers is much smaller than that introduced by the synthesizers, and, therefore, the frequency division approach is typically used. In the actual application process, integer frequency division is usually chosen.

The aliasing signal generated by the ADC sampling of the pilot-tone signal interferes with the beat-note frequency measurement. For example, when the sampling frequency of the ADC is 82 MHz and the frequency of the pilot-tone signal is 80 MHz, the frequency of the aliased signal generated by the ADC in the under-sampled pilot-tone signal will be 2 MHz. Therefore, the frequency of the aliased signal must not overlap the beat-note frequency range. This constraint can be expressed by the following equation:

$$|f_{\text{ADC}} - f_{\text{PT}}| < f_{\text{lower}}. \quad (7)$$

Therefore, setting the pilot-tone signal frequency f_{PT} and ADC sampling frequency f_{ADC} imposes the following constraints:

$$\left\{ \begin{array}{l} n_1 * f_{\text{ADC}} = f_{\text{USO}} \\ n_2 * f_{\text{PT}} = f_{\text{USO}} \\ f_{\text{ADC}} > 2f_{\text{upper}} \\ |f_{\text{ADC}} - f_{\text{PT}}| < f_{\text{lower}} \\ f_{\text{USO}} < 5 \text{ GHz} \\ f_{\text{PT}} < 98 \text{ MHz} \end{array} \right. \quad n_1, n_2 \text{ are integers}, \quad (8)$$

where the value of 5 GHz is the artificial upper bound set for f_{USO} to constrain it to finite values. Based on Kullmann's [15] study, the upper bound of f_{PT} is set to 98 MHz to avoid poor performance of the pilot tone correction.

3. Hierarchical Optimization Algorithm

In this section, the optimization model is introduced in Section 3.1, and then the hierarchical optimization algorithm for this optimization model is introduced in Section 3.2.

3.1. Optimization Model

According to the analysis in Section 2, the frequency of the mission operation involves four terms: the beat-note f_{het} , the USO f_{USO} , the pilot-tone signal f_{PT} , and the ADC sampling f_{ADC} frequencies. The variable f_{het} is affected by the Doppler shift and changes dynamically over time, while the remaining three terms remain unchanged. The variation range of the inter-satellite beat-note frequency f_{het} is determined by the lower and upper bounds of the beat-note frequency, namely f_{lower} , and f_{upper} . Therefore, the optimization goal is to make the sideband readout displacement noise meet the mission requirement, minimize the total readout displacement noise, and maximize the feasible range of beat-

note frequency by reasonably allocating the values of each frequency or frequency band, and modulation depth m , respectively. The optimization model is as follows:

$$\begin{aligned}
 \Gamma_1(f_{\text{upper}}, f_{\text{USO}}, f_{\text{PT}}, f_{\text{ADC}}, m, P_{\text{local}}) &= \min(\delta x^{\text{total}}) \\
 \Gamma_2(f_{\text{upper}}, f_{\text{lower}}) &= \max(f_{\text{upper}} - f_{\text{lower}}) \\
 \text{s.t.} & \\
 &\left\{ \begin{array}{l} \delta x^{\text{sideband}} < \frac{1}{10} \delta x^{\text{total}} \\ n_1 * f_{\text{ADC}} = f_{\text{USO}} \\ n_2 * f_{\text{PT}} = f_{\text{USO}} \\ f_{\text{ADC}} > 2f_{\text{upper}} \\ |f_{\text{ADC}} - f_{\text{PT}}| < f_{\text{lower}} \\ f_{\text{lower}} \geq 2 \text{ MHz} \\ f_{\text{upper}} \leq 25 \text{ MHz} \\ f_{\text{USO}} < 5 \text{ GHz} \\ f_{\text{PT}} < 98 \text{ MHz} \\ 0.44 < m < 0.61 \end{array} \right. \quad n_1, n_2 \text{ are integers,} \tag{9}
 \end{aligned}$$

where Γ_1 and Γ_2 represent the two objective functions.

3.2. Optimization Process

Owing to the multiple objectives and parameters involved in the optimization solution, a hierarchical optimization approach is used for this optimization model based on computational efficiency considerations when selecting $f_{\text{USO}}, f_{\text{PT}}, f_{\text{ADC}}, f_{\text{upper}}, f_{\text{lower}}$, and m . The optimization process is as follows.

Step 1: A multi-objective optimization algorithm is used to set the lower and upper bounds of the beat-note frequency ($f_{\text{lower}}, f_{\text{upper}}$), USO frequency f_{USO} , and sideband modulation depth m . The multi-objective optimization model for this step is expressed by Equation (10).

$$\begin{aligned}
 &\left\{ \begin{array}{l} \Gamma_1(f_{\text{upper}}, f_{\text{USO}}, \overline{f_{\text{PT}}}, \overline{f_{\text{ADC}}}, m, \overline{P_{\text{local}}}) = \min(\delta x^{\text{total}}) \\ \Gamma_2(f_{\text{lower}}) = \max(f_{\text{lower}}) \\ \Gamma_3(f_{\text{upper}}) = \min(f_{\text{upper}}) \\ \Gamma_4(f_{\text{upper}}, f_{\text{lower}}) = \max(f_{\text{upper}} - f_{\text{lower}}) \end{array} \right. \tag{10} \\
 \text{s.t.} & \\
 &\left\{ \begin{array}{l} 0.44 < m < 0.61 \\ f_{\text{USO}} < 5 \text{ GHz} \\ 2 \text{ MHz} < f_{\text{lower}} < 10 \text{ MHz} \\ 20 \text{ MHz} < f_{\text{upper}} \leq 25 \text{ MHz} \end{array} \right.
 \end{aligned}$$

In Equation (10), Γ_x denotes the x-th optimization objective. In Γ_1 , where $\overline{f_{\text{PT}}}, \overline{f_{\text{ADC}}}$ and $\overline{P_{\text{local}}}$ denote that the variables are taken as constant. Γ_2 and Γ_3 in Equation (10) are the two objective functions derived from Γ_1 in Equation (9) according to Equations (3) and (8), respectively. Γ_2 aims to expand the selection spaces of f_{ADC} and f_{PT} , and Γ_3 aims to reduce the sideband readout displacement noise, which is proportional to f_{upper} . The objective function Γ_4 aims to maximize the feasible range of the beat-note frequency, which is the opposite of Γ_2 and Γ_3 . In actual mission operations, $f_{\text{upper}}, f_{\text{lower}}$, and f_{USO} are commonly

set as integers. To reduce the complexity of the optimization problem while determining the solution, f_{upper} , f_{lower} , and f_{USO} are not constrained as integers in this step.

In the current Taiji program, the upper bound of the beat-note frequency is 25 MHz. Using the parameter values listed in Table 1, $P_{\text{receive}} = 2.154 \times 10^{-9}$ W. Therefore, the values of all parameters in Equation (4), except P_{local} , are obtained. Because P_{local} appears in both the numerator and denominator, the optimal value of P_{local} , which is 2.06×10^{-3} W in the current parameter settings, can be derived by simply minimizing. When calculating δx^{total} in this step, the values of $P_{\text{local}} = 2.06 \times 10^{-3}$ W and the parameters in Table 1 are used by default.

Step 2: The values of f_{lower} , f_{upper} , and f_{USO} obtained in Step 1 are adjusted to be integers:

$$\begin{cases} f_{\text{lower}}^{\text{new}} = \text{floor}(f_{\text{lower}}) \\ f_{\text{upper}}^{\text{new}} = \text{floor}(f_{\text{upper}}) \\ f_{\text{USO}}^{\text{new}} = \text{floor}(f_{\text{USO}}) \end{cases}, \quad (11)$$

where $f_{\text{lower}}^{\text{new}}$, $f_{\text{upper}}^{\text{new}}$, and $f_{\text{USO}}^{\text{new}}$ represent the adjusted values of f_{lower} , f_{upper} , and f_{USO} , respectively.

Step 3: Exhaustive enumeration is used to search for possible $[f_{\text{USO}}, f_{\text{PT}}, f_{\text{ADC}}]$ combinations. The values of f_{PT} and f_{ADC} need to satisfy the following constraints:

$$\begin{cases} f_{\text{ADC}} >= 2f_{\text{upper}}^{\text{new}} \\ 1 < |f_{\text{ADC}} - f_{\text{PT}}| < f_{\text{lower}}^{\text{new}} \end{cases}. \quad (12)$$

Suppose there are n possible combinations stored in the following matrix:

$$\begin{bmatrix} f_{\text{USO}}^1, f_{\text{PT}}^1, f_{\text{ADC}}^1 \\ f_{\text{USO}}^2, f_{\text{PT}}^2, f_{\text{ADC}}^2 \\ \dots \\ f_{\text{USO}}^n, f_{\text{PT}}^n, f_{\text{ADC}}^n \end{bmatrix} \quad (13)$$

The combination such that f_{USO}^j , $j = 1, 2, \dots, n$ is closest to $f_{\text{USO}}^{\text{new}}$ is chosen. If f_{USO}^m is closest to $f_{\text{USO}}^{\text{new}}$, then $f_{\text{USO}}^{\text{new}} = f_{\text{USO}}^m$ is updated. To distinguish this value from $f_{\text{USO}}^{\text{new}}$ obtained in Step 2, the updated $f_{\text{USO}}^{\text{new}}$ obtained in this step is referred to as $f_{\text{USO}}^{\text{opt}}$.

Step 4: P_{local} is updated according to $f_{\text{upper}}^{\text{new}}$, and then the modulation depth m is updated according to $[f_{\text{upper}}^{\text{new}}, f_{\text{USO}}^{\text{opt}}]$ from Steps 2 and 4. The updating method is as follows:

$$\begin{cases} \min(\delta\phi_{\text{SN}}^2 + \delta\phi_{\text{RIN}}^2 + \delta\phi_{\text{EN}}^2) \\ \left\{ \begin{array}{l} f_{\text{upper}} = f_{\text{upper}}^{\text{new}} \\ P_{\text{receive}} = 2.154 \times 10^{-9} \text{ W} \end{array} \right. \\ \min(\delta x^{\text{total}}(f_{\text{USO}}^{\text{opt}}, f_{\text{upper}}^{\text{new}}, m)) \\ \left\{ \begin{array}{l} \delta x^{\text{total}}(f_{\text{USO}}^{\text{opt}}, f_{\text{upper}}^{\text{new}}, m) = \delta x^{\text{total}}\left(\frac{f_{\text{upper}}^{\text{new}}}{f_{\text{USO}}^{\text{opt}}} \frac{1}{J_1(m)^2} + \frac{1}{J_0(m)^2}\right) \\ m \in [0.44, 0.61] \end{array} \right. \end{cases} \quad (14)$$

The minimum value of the total readout displacement noise after updating $[f_{\text{upper}}^{\text{new}}, f_{\text{USO}}^{\text{opt}}]$ is obtained by adjusting the parameter m in the range $[0.44, 0.61]$.

Step 5: Backtracking mechanism. Since the default P_{local} value is obtained by assuming $f_{\text{upper}} = 25$ MHz, it may change after completing Steps 1–4. Therefore, if P_{local} changed, then update P_{local} and return to Step 1 until no new P_{local} appears.

The flowchart of the algorithm as shown in Figure 2.

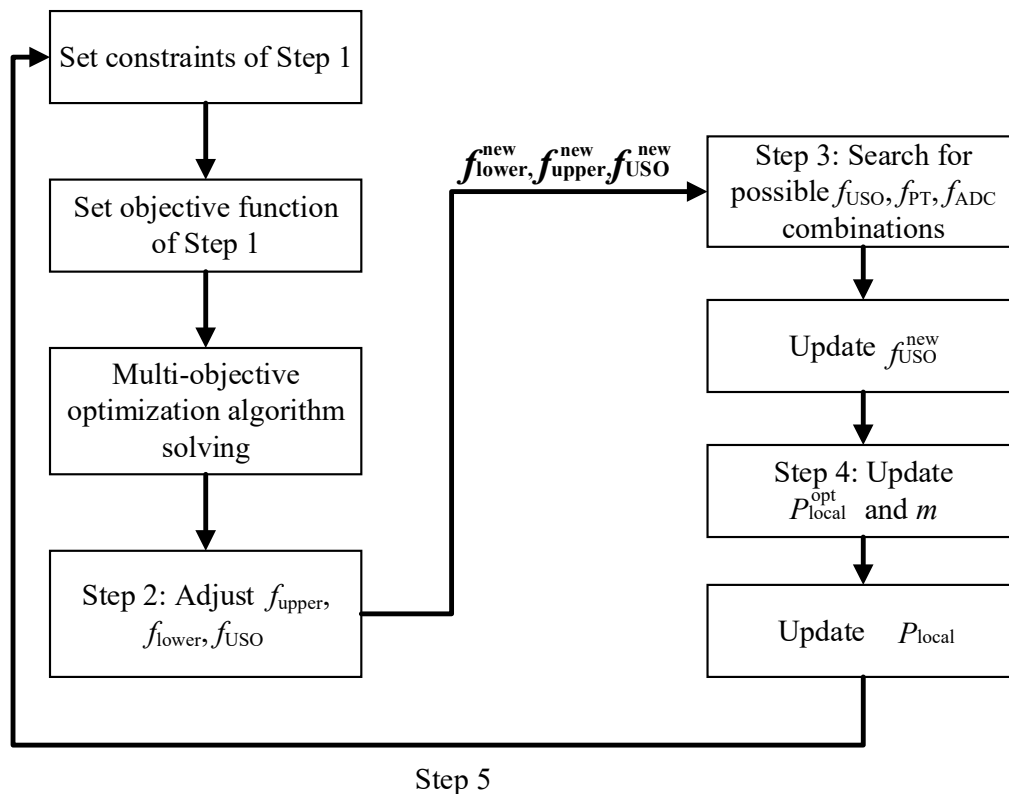


Figure 2. Flowchart of the algorithm.

4. Results and Discussion

4.1. Optimization Results

The mathematical model presented in Section 3 was solved using an AMD Ryzen 9 3900X 12-core processor. The time consumption of each step is listed in Table 2. To reduce the complexity associated with the solution of multi-objective problems and improve the convergence efficiency of the solution set, we used one of the most popular multi-objective optimization algorithms: the nondominated sorting genetic algorithm II (NSGA-II) [24].

Table 2. Time consumption of each step.

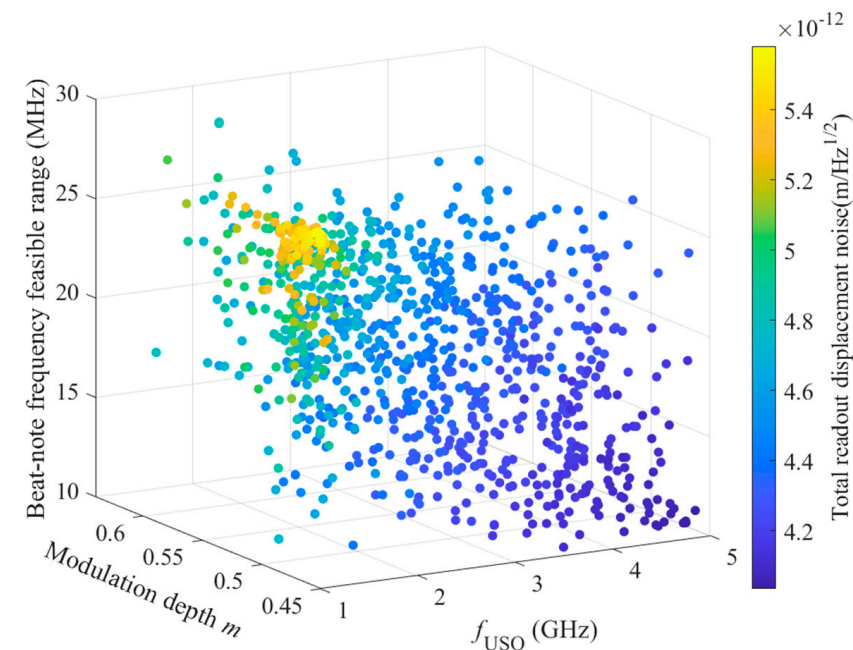
Steps	Algorithm	Time Consumption
Step 1	Nondominated sorting genetic algorithm II [24]	240 s
Step 2	Round	0.005 s
Step 3	Exhaustive enumeration	1 s
Step 4	Optimization	0.03 s

As a characteristic of multi-objective optimization algorithms, an optimal solution set is usually obtained instead of a single optimal solution to balance the degree of optimization of each objective.

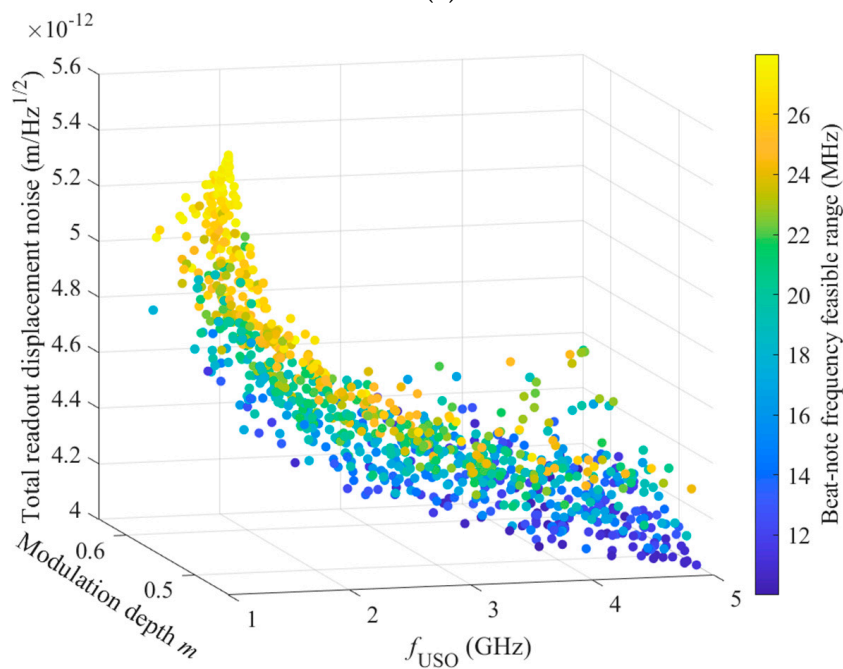
The Pareto-optimal solution plane obtained in Step 1 of Section 3.2 is shown in Figure 3.

During the operation of a mission, a smaller total readout displacement noise δx^{total} indicates a better detection of signals, and a larger feasible range of the beat-note frequency, which exists between f_{upper} and f_{lower} , indicates a better offset frequency setting. In Figure 3a, the warmer the color of the scatter plot, the higher the value of δx^{total} . Hence, the smaller the value of the beat-note frequency range, the smaller the value of the modulation depth; a larger value of f_{USO} corresponds to a smaller value of δx^{total} . In Figure 3b, a

warmer scatter color indicates a larger beat-note frequency interval; a larger beat-note frequency range corresponds to a larger δx^{total} value. Based on Figure 3, we can conclude that the value of the beat-note frequency range is inversely related to the magnitude of δx^{total} . The two targets need to be reasonably balanced via optimization to increase the maximum feasible range of the beat-note frequency and decrease δx^{total} .



(a)



(b)

Figure 3. Pareto-optimal solution plane: (a) Scatter plot of the total readout displacement noise with the modulation depth; USO frequency; and beat-note frequency in a feasible range along the x-, y-, and z-axes, respectively. The total readout displacement noise δx^{total} is represented by the colored bar. (b) Scatter plot of the beat-note frequency in a feasible range with the modulation depth; USO frequency; and total readout displacement noise along the x-, y-, and z-axes, respectively. The beat-note frequency in a feasible range is represented by the colored bar.

This planning problem was solved based on the optimization algorithm introduced in Section 3.2. The results of the 20 Pareto-optimal (feasible) solutions obtained from the final solution are listed in Table 3. The units of f_{lower} , f_{upper} , f_{ADC} , f_{PT} , and f_{USO} are MHz, and the total readout displacement noise δx^{total} has units of $\text{pm}/\sqrt{\text{Hz}}$. It is worth noting that these are the optimal 20 solutions by balancing the two optimization objectives.

Table 3. Pareto-optimal feasible solutions obtained from hierarchical optimization algorithm.

Number	f_{lower} (MHz)	f_{upper} (MHz)	Feasible Range	f_{ADC} (MHz)	f_{PT} (MHz)	f_{USO} (MHz)	m	δx^{total} ($\text{pm}/\sqrt{\text{Hz}}$)	P_{local} (mW)
1	3	25	23	92	90	4140	0.44	4.21	2.06
2	3	25	23	63	61	3843	0.44	4.23	2.06
3	3	25	23	68	66	2244	0.48	4.47	2.06
4	3	25	23	62	60	1860	0.50	4.57	2.06
5	3	24	22	84	82	3444	0.44	4.24	1.99
6	4	25	22	71	68	4828	0.44	4.16	2.06
7	4	25	22	70	67	4690	0.44	4.17	2.06
8	3	24	22	65	63	4095	0.44	4.18	1.99
9	4	25	22	88	86	3784	0.44	4.24	2.06
10	4	25	22	59	57	3363	0.44	4.28	2.06
11	4	25	22	59	57	3363	0.44	4.28	2.06
12	4	25	22	70	68	2380	0.48	4.44	2.06
13	4	25	22	58	56	1624	0.52	4.65	2.06
14	3	23	21	96	94	4512	0.44	4.12	1.92
15	3	23	21	61	59	3599	0.44	4.19	1.92
16	4	24	21	65	62	4030	0.44	4.19	1.99
17	4	24	21	84	82	3444	0.44	4.24	1.99
18	4	24	21	88	86	3784	0.44	4.21	1.99
19	3	23	21	60	58	1740	0.50	4.52	1.92
20	5	25	21	59	57	3363	0.44	4.28	2.06

The results in Table 3 show that, after utilizing the proposed algorithm, the maximum beat-note frequency feasible range is 23 MHz and yields a total readout displacement noise of $4.21 \text{ pm}/\sqrt{\text{Hz}}$, which corresponds to the parameter combination $(f_{\text{lower}}, f_{\text{upper}}, f_{\text{ADC}}, f_{\text{PT}}, f_{\text{USO}}, m) = (3 \text{ MHz}, 25 \text{ MHz}, 92 \text{ MHz}, 90 \text{ MHz}, 4140 \text{ MHz}, 0.44)$. Additionally, the smallest total readout displacement noise was $4.12 \text{ pm}/\sqrt{\text{Hz}}$, which corresponds to $(f_{\text{lower}}, f_{\text{upper}}, f_{\text{ADC}}, f_{\text{PT}}, f_{\text{USO}}, m) = (3 \text{ MHz}, 23 \text{ MHz}, 96 \text{ MHz}, 94 \text{ MHz}, 4512 \text{ MHz}, 0.44)$. From Equation (4), different f_{upper} values correspond to different optimal P_{local} values. Therefore, when $f_{\text{upper}} = 23 \text{ MHz}$, $P_{\text{local}} = 1.92 \text{ mW}$, and $f_{\text{upper}} = 24 \text{ MHz}$, we obtain $P_{\text{local}} = 1.99 \text{ mW}$, $f_{\text{upper}} = 25 \text{ MHz}$, and $P_{\text{local}} = 2.06 \text{ mW}$.

According to Taiji mission budget, the position noise is $8 \text{ pm}/\sqrt{\text{Hz}}$ [6], which includes laser frequency noise, readout displacement noise, laser pointing noise, tilt-to-length noise, and so on. Among them, the frequency stability is $30 \text{ Hz}/\sqrt{\text{Hz}}$, the limit of is laser-pointing noise and tile-to-length noise is $1 \text{ pm}/\sqrt{\text{Hz}}$ [25], and the readout displacement noise is about $7.5 \text{ pm}/\sqrt{\text{Hz}}$ [26]. After parameter optimization, the total readout displacement noise is reduced to $4.12 \text{ pm}/\sqrt{\text{Hz}}$. The sensitivity curve of Taiji program detection limit and after optimization with other noise budgets the same, is shown Figure 4. It can be seen from the figure that the optimized parameters have improved the sensitivity in the range of 10 mHz–1 Hz.

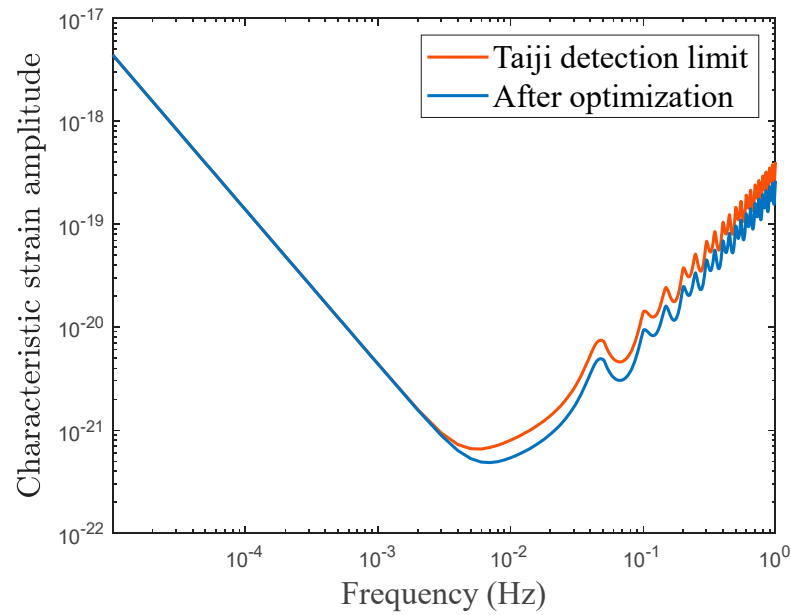


Figure 4. The sensitivity curve of the Taiji program detection limit (red) and after optimization (blue).

4.2. Experimental Adjustment of P_{tel} and f_{upper}

According to Equation (5), the value of $P_{receive}$ is positively proportional to P_{tel} . The optimal value of P_{local} is directly influenced by f_{upper} . To describe the effect of the values of P_{tel} and f_{upper} on $P_{receive}$ and P_{local} in a more intuitive manner, we conducted the following experiments: (1) vary the value of P_{tel} in the range [2 W, 3 W] with an interval of 0.1 W and observe the variations of $P_{receive}$ and total readout displacement noise; and (2) vary the value of f_{upper} in the range [20 MHz, 30 MHz] with an interval of 1 MHz and observe the variations of the optimal P_{local} value and minimum total readout displacement noise δx^{total} . The results are shown in Figures 5 and 6. It should be noted that in the first experiment, other parameters such as P_{local} , m , and f_{upper} were set according to the first optimization results shown in Table 3, while in the second experiment, we set $P_{tel} = 2$ W.

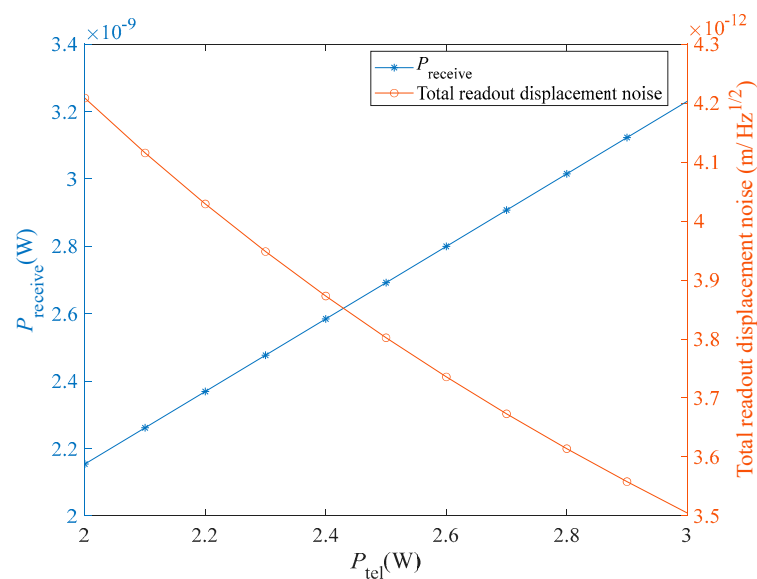


Figure 5. Variation of $P_{receive}$ and the total readout displacement noise as a function of P_{tel} . The x-, left-hand y-, and right-hand y-axes show P_{tel} , $P_{receive}$, and the total readout displacement noise, respectively.

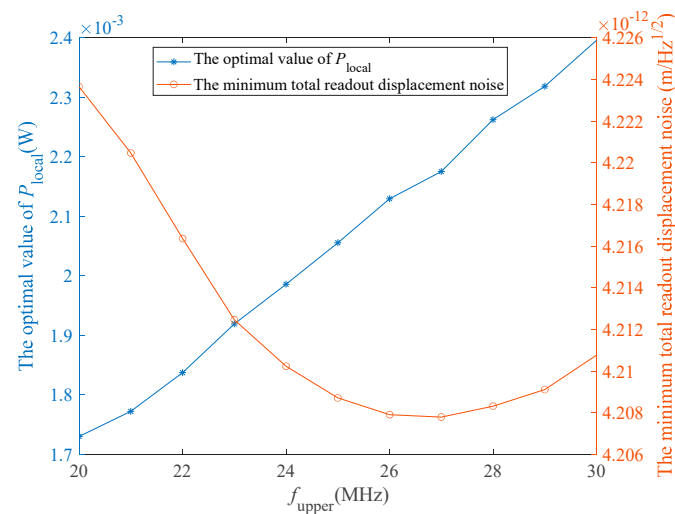


Figure 6. Variations of the optimal P_{local} value and the minimum total readout displacement noise with f_{upper} . The x-, left-hand y-, and right-hand y-axes show f_{upper} , the optimal P_{local} , and the minimum total readout displacement noise, respectively.

In Figure 5, as P_{tel} increases, $P_{receive}$ increases linearly, and δx^{total} decreases approximately linearly. In Equation (4) and Step 5 of the optimization algorithm proposed in this study, the variation of $P_{receive}$ may cause a change in the optimal P_{local} value. However, in practice, the variation of $P_{receive}$ is so small that it barely affects the optimal value of P_{local} . Figure 6 shows the variations of P_{local} and δx^{total} with f_{upper} . The optimal value of P_{local} increases as f_{upper} increases, while δx^{total} first decreases and then increases. When $f_{upper} = 27$ MHz, the optimal P_{local} value is 2.175 mW, and δx^{total} has its smallest value of 4.2078 pm/ $\sqrt{\text{Hz}}$.

In actual mission operations, a larger value of $P_{receive}$ can not only reduce δx^{total} , but also reduce the difficulty of weak-light phase-locked loops to some extent [27], which means that the power of P_{tel} must be increased. However, increasing P_{tel} undoubtedly increases the difficulty of the design of the devices associated with this system, and therefore, a trade-off needs to be made considering the practical applications of this system. In addition, different upper bounds of the beat-note frequency correspond to different optimal values of P_{local} , and different minimum total readout displacement noise values. The value of P_{local} can be set by referring to Figure 6.

5. Conclusions

In this study, a hierarchical optimization algorithm is proposed to solve the Taiji program's system-level frequency setting scheme. The optimization model considered the effects of six main factors, namely f_{lower} , f_{upper} , f_{ADC} , f_{PT} , f_{USO} , and m . Two optimization objectives were used, including minimizing the total readout displacement noise and maximizing the feasible beat-note frequency range. Considering the characteristics involved in solving multi-objective optimization problems, 20 Pareto-optimal solutions were obtained. The minimum total readout displacement noise was 4.12 pm/ $\sqrt{\text{Hz}}$, which corresponded to a beat-note frequency feasible range of 21 MHz, with $(f_{lower}, f_{upper}, f_{ADC}, f_{PT}, f_{USO}, m) = (3 \text{ MHz}, 23 \text{ MHz}, 96 \text{ MHz}, 94 \text{ MHz}, 4512 \text{ MHz}, 0.44)$. The maximum feasible range of the beat-note frequency was 23 MHz with a total readout displacement noise of 4.21 pm/ $\sqrt{\text{Hz}}$, with $(f_{lower}, f_{upper}, f_{ADC}, f_{PT}, f_{USO}, m) = (3 \text{ MHz}, 25 \text{ MHz}, 92 \text{ MHz}, 90 \text{ MHz}, 4140 \text{ MHz}, 0.44)$. Hence, different values of the parameters f_{upper} , f_{ADC} , f_{PT} , and f_{USO} result in different final optimization results. Therefore, these two objectives were not simultaneously optimized, and a trade-off between these two objectives needs to be made in practical applications of this system. Moreover, we analyzed the effects of P_{tel} and f_{upper} on $P_{receive}$ and P_{local} , and then explored the effects of

these two factors on the total readout displacement noise. The results provide a reference for setting the frequency setting strategy during laser transmission and readout, determining the power ratio between the sidebands and carrier and selecting the relevant equipment parameters of laser interferometry systems in the Taiji program.

Author Contributions: Conceptualization, X.M., Z.Y. and X.P.; methodology, J.Z., C.G. and M.Z.; validation, X.M., Z.Y. and X.P.; writing—original draft preparation, J.Z. and X.M.; writing—review and editing, X.M., Z.Y. and W.T. All authors have read and agreed to the published version of the manuscript.

Funding: This research was funded by the National Key Research and Development Program of China (Grant No. 2020YFC2200100) and the Chinese Academy of Sciences Strategic Pioneer Program on Space Science (Grant No. XDA1502110201).

Institutional Review Board Statement: Not applicable.

Informed Consent Statement: Not applicable.

Data Availability Statement: Data underlying the results presented in this paper are not publicly available at this time but may be obtained from the authors upon reasonable request.

Acknowledgments: We would like to thank Ziren Luo and Heshan Liu in Institute of Mechanics for the helpful discussion.

Conflicts of Interest: The authors declare no conflict of interest.

References

1. Abramovici, A.; Althouse, W.E.; Drever, R.W.; Gürsel, Y.; Kawamura, S.; Raab, F.J.; Shoemaker, D.; Sievers, L.; Spero, R.E.; Thorne, K.S. LIGO: The Laser Interferometer Gravitational-Wave Observatory. *Science* **1992**, *256*, 325–333. [[CrossRef](#)] [[PubMed](#)]
2. Thorne, K.S. Gravitational Waves. *arXiv* **1995**, arXiv:gr-qc/9506086.
3. Hough, J.; Robertson, D.; Ward, H.; McNamara, P. LISA—The Interferometer. *Adv. Space Res.* **2003**, *32*, 1247–1250. [[CrossRef](#)]
4. Danzmann, K.; Prince, T.A.; Binetruy, P.; Bender, P.; Buchman, S.; Centrella, J.; Cerdonio, M.; Cornish, N.; Cruise, M.; Cutler, C.J. LISA: Unveiling a Hidden Universe. In *Assessment Study Report ESA/SRE*; AEI: Hannover, Germany, 2011; Volume 3.
5. Hu, W.; Wu, Y. The Taiji Program in Space for Gravitational Wave Physics and the Nature of Gravity. *Natl. Sci. Rev.* **2017**, *4*, 685–686. [[CrossRef](#)]
6. Li, Y.; Jin, G. A Brief Overview of 8 m Prototype Facility of Laser Interferometer for Taiji Pathfinder Mission. *Appl. Phys. B* **2021**, *127*, 88. [[CrossRef](#)]
7. Luo, Z.; Guo, Z.; Jin, G.; Wu, Y.; Hu, W. A Brief Analysis to Taiji: Science and Technology. *Results Phys.* **2020**, *16*, 102918. [[CrossRef](#)]
8. Luo, J.; Chen, L.-S.; Duan, H.-Z.; Gong, Y.-G.; Hu, S.; Ji, J.; Liu, Q.; Mei, J.; Milyukov, V.; Sazhin, M.; et al. TianQin: A Space-Borne Gravitational Wave Detector. *Class. Quantum Grav.* **2016**, *33*, 035010. [[CrossRef](#)]
9. Otto, M. Time-Delay Interferometry Simulations for the Laser Interferometer Space Antenna. Ph.D. Thesis, Gottfried Wilhelm Leibniz Universität Hannover, Hannover, Germany, 2015.
10. Brause, N.C. Auxiliary Function Development for the LISA Metrology System. Ph.D. Thesis, Gottfried Wilhelm Leibniz Universität Hannover, Hannover, Germany, 2018.
11. Chiow, S.; Williams, J.; Yu, N. Laser-Ranging Long-Baseline Differential Atom Interferometers for Space. *Phys. Rev. A* **2015**, *92*, 063613. [[CrossRef](#)]
12. Wang, Y. On Inter-Satellite Laser Ranging, Clock Synchronization and Gravitational Wave Data Analysis. Ph.D. Thesis, Gottfried Wilhelm Leibniz Universität Hannover, Hannover, Germany, 2014.
13. Barke, S. Inter-Spacecraft Frequency Distribution. Ph.D. Thesis, Gottfried Wilhelm Leibniz Universität Hannover, Hannover, Germany, 2015.
14. Pollack, S.E.; Stebbins, R.T. A Demonstration of LISA Laser Communication. *Class. Quantum Grav.* **2006**, *23*, 4201–4213. [[CrossRef](#)]
15. Kullmann, J. Development of a Digital Phase Measuring System with Microradian Precision for LISA. Ph.D. Thesis, Gottfried Wilhelm Leibniz Universität Hannover, Hannover, Germany, 2012.
16. Zhang, J.; Yang, Z.; Ma, X.; Peng, X.; Liu, H.; Tang, W.; Zhao, M.; Gao, C.; Qiang, L.-E.; Han, X.; et al. Inter-Spacecraft Offset Frequency Setting Strategy in the Taiji Program. *Appl. Opt.* **2022**, *61*, 837–843. [[CrossRef](#)] [[PubMed](#)]
17. Heinzl, G.; Esteban, J.J.; Barke, S.; Otto, M.; Wang, Y.; Garcia, A.F.; Danzmann, K. Auxiliary Functions of the LISA Laser Link: Ranging, Clock Noise Transfer and Data Communication. *Class. Quantum Grav.* **2011**, *28*, 094008. [[CrossRef](#)]
18. Klipstein, W.; Halverson, P.G.; Peters, R.; Cruz, R.; Shaddock, D. Clock Noise Removal in LISA. In *Proceedings of the Laser Interferometer Space Antenna: 6th International LISA Symposium*, Greenbelt, MD, USA, 19–23 June 2006; Volume 873, pp. 312–318.
19. Barke, S.; Brause, N.; Bykov, I.; Esteban Delgado, J.J.; Enggaard, A.; Gerberding, O.; Heinzl, G.; Kullmann, J.; Pedersen, S.M.; Rasmussen, T. *LISA Metrology System—Final Report*; AEI: Hannover, Germany, 2014.

20. Li, Y.; Wang, C.; Wang, L.; Liu, H.; Jin, G. A Laser Interferometer Prototype with Pico-Meter Measurement Precision for Taiji Space Gravitational Wave Detection Mission in China. *Microgravity Sci. Technol.* **2020**, *32*, 331–338. [[CrossRef](#)]
21. Ren, Z.; Jun, Z.; Jiqiao, L.; Dijun, C.; Yan, Y.; Weibiao, C. Solid State Tunable Single-Frequency Laser Based on Non-Planar Ring Oscillator. *Chin. J. Lasers* **2011**, *38*, 1102011. [[CrossRef](#)]
22. Gao, R.; Liu, H.; Zhao, Y.; Luo, Z.; Jin, G. Automatic, High-Speed, High-Precision Acquisition Scheme with QPD for the Taiji Program. *Opt. Express* **2021**, *29*, 821. [[CrossRef](#)] [[PubMed](#)]
23. Zhao, Y. *The Research on the Tilt to Length Coupling Noise in Inter-Satellite Interference Link for the Space-Based Gravitational Wave Detection*; Chinese Academy of Sciences: Beijing, China, 2021.
24. Deb, K.; Pratap, A.; Agarwal, S.; Meyarivan, T. A Fast and Elitist Multiobjective Genetic Algorithm: NSGA-II. *IEEE Trans. Evol. Comput.* **2002**, *6*, 182–197. [[CrossRef](#)]
25. Luo, Z.; Wang, Y.; Wu, Y.; Hu, W.; Jin, G. The Taiji Program: A Concise Overview. *Prog. Theor. Exp. Phys.* **2021**, *2021*, 05A108. [[CrossRef](#)]
26. Liu, H.; Li, Y.; Jin, G. Numerical Simulations of Arm-Locking for Taiji Space Gravitational Waves Detection. *Microgravity Sci. Technol.* **2021**, *33*, 41. [[CrossRef](#)]
27. Wan, C. A Study on nW-Level Weak Light Optical Phase-Locking Techniques. Master's Thesis, Huazhong University of Science and Technology, Wuhan, China, 2012.

Disclaimer/Publisher's Note: The statements, opinions and data contained in all publications are solely those of the individual author(s) and contributor(s) and not of MDPI and/or the editor(s). MDPI and/or the editor(s) disclaim responsibility for any injury to people or property resulting from any ideas, methods, instructions or products referred to in the content.